Ultrasonics Sonochemistry 90 (2022) 106222

Contents lists available at ScienceDirect

Ultrasonics Sonochemistry

journal homepage: www.elsevier.com/locate/ultson

Thermally-enhanced sono-photo-catalysis by defect and facet modulation of Pt-TiO_2 catalyst for high-efficient hydrogen evolution

Rong Ma [a,1], Hui Su [a,1], Jie Sun [a,b,*], Donghui Li [a], Zhenwen Zhang [a], Jinjia Wei [a]

[a] School of Chemical Engineering and Technology, Xi'an Jiaotong University, Xi'an 710049, China
[b] Adv Energy Sci & Technol Guangdong Lab, Foshan Xianhu Lab, Xianhu Hydrogen Valley 528200, Foshan, China

ARTICLE INFO

Keywords:
Sono-photo-catalysis (SPC)
Thermal effect
Hydrogen evolution
Defect engineering
Facet control

ABSTRACT

Sono-photo-catalysis (SPC) has been regarded as a promising route for hydrogen evolution from water splitting due to the sono-photo-synergism, whereas its current performance (~μmol g^{-1} h^{-1}) is yet far from expectation. Herein, we give the first demonstration that the intrinsically coupled thermal effects of light and ultrasound, which is normally underestimated or neglected, can simultaneously reshape the photo- and sono-catalytic activities for hydrogen evolution and establish a higher degree of synergy between light and ultrasound in SPC even on the traditional Pt-TiO_2 catalyst. A high-efficient hydrogen evolution rate of 225.04 mmol g^{-1} h^{-1} with light-to-hydrogen efficiency of 0.89% has been achieved in thermally-enhanced SPC, which is an order of magnitude higher than that without thermal effects. More impressively, the increase of synergy index up to 53% has been achieved. Through experiments and theoretical calculations, the thermally-enhanced sono-photo-synergism is attributed to the sono-photo-thermo-modulated structural optimization of defect-rich TiO_2 support and deaggregated Pt species with functional complementary lattice facets, which optimizes not only the thermodynamic properties by enhancing light harvesting and the charge redox power, but also the kinetic properties by accelerating the net efficiency of charge separation and the whole processes of water splitting, including the dissociation of water molecules on high-index (200) Pt facets and production of H* intermediates on defect-rich TiO_{2-x} support and low-index (111) Pt facets. This study exemplifies that coupling light- and ultrasonic-induced thermal effects in SPC system could enhance the synergy between light and ultrasound by modulating catalyst structure to achieve double optimization of thermodynamic and kinetic properties of SPC hydrogen evolution.

1. Introduction

Efficient hydrogen evolution technology is necessary for realizing the transformation from fossil fuel to clean energy [1]. As a straightforward pathway for solar energy to hydrogen energy conversion, photocatalytic (PC) technology potentially enables much simpler and more economically competitive systems [2]. However, it yet remains unsatisfactory mainly due to two aspects: (1) The intrinsically thermodynamic challenges, such as the mismatch between suitable band gap and redox potential with sufficient driving force to inevitably confront the extending light absorption accompanied with decreasing driving force based on the narrowing band gap [3,5–11]; (2) The typically kinetic limitations, including the fast recombination of photo-generated electrons and holes to reduce the number of electrons participating in the PC hydrogen proton reduction, and the inappropriate adsorption/desorption properties of multiple reactants/intermediates [3–11]. Therefore, it is urgently required to develop a more effective route to tackle the above-mentioned issues.

As a flexible and controllable strategy, sono-photo-catalytic (SPC) technology has attracted more and more research interests in degradation of environmental pollutants due to the unique advantage of ultrasound as an additional impetus to enhance PC activity [12], which makes us aware of the great potential of SPC technology in overcoming the above-mentioned challenges. In principle, ultrasound could optimize the thermodynamic and kinetic properties of PC reaction through acoustic cavitation and associated acoustic streaming [15]. On the one hand, acoustic cavitation induces localized supercritical conditions by the nucleation, growth and subsequent collapse of bubbles to create numerous high temperature (~5500 K) and high pressure (~500 atm) "micro-reactors" [13], resulting in favorable thermodynamic condition

* Corresponding author at: School of Chemical Engineering and Technology, Xi'an Jiaotong University, Xi'an 710049, China.
E-mail address: sunjie@xjtu.edu.cn (J. Sun).
[1] These authors contributed equally to this work.

https://doi.org/10.1016/j.ultsonch.2022.106222
Received 12 July 2022; Received in revised form 29 October 2022; Accepted 2 November 2022
Available online 8 November 2022

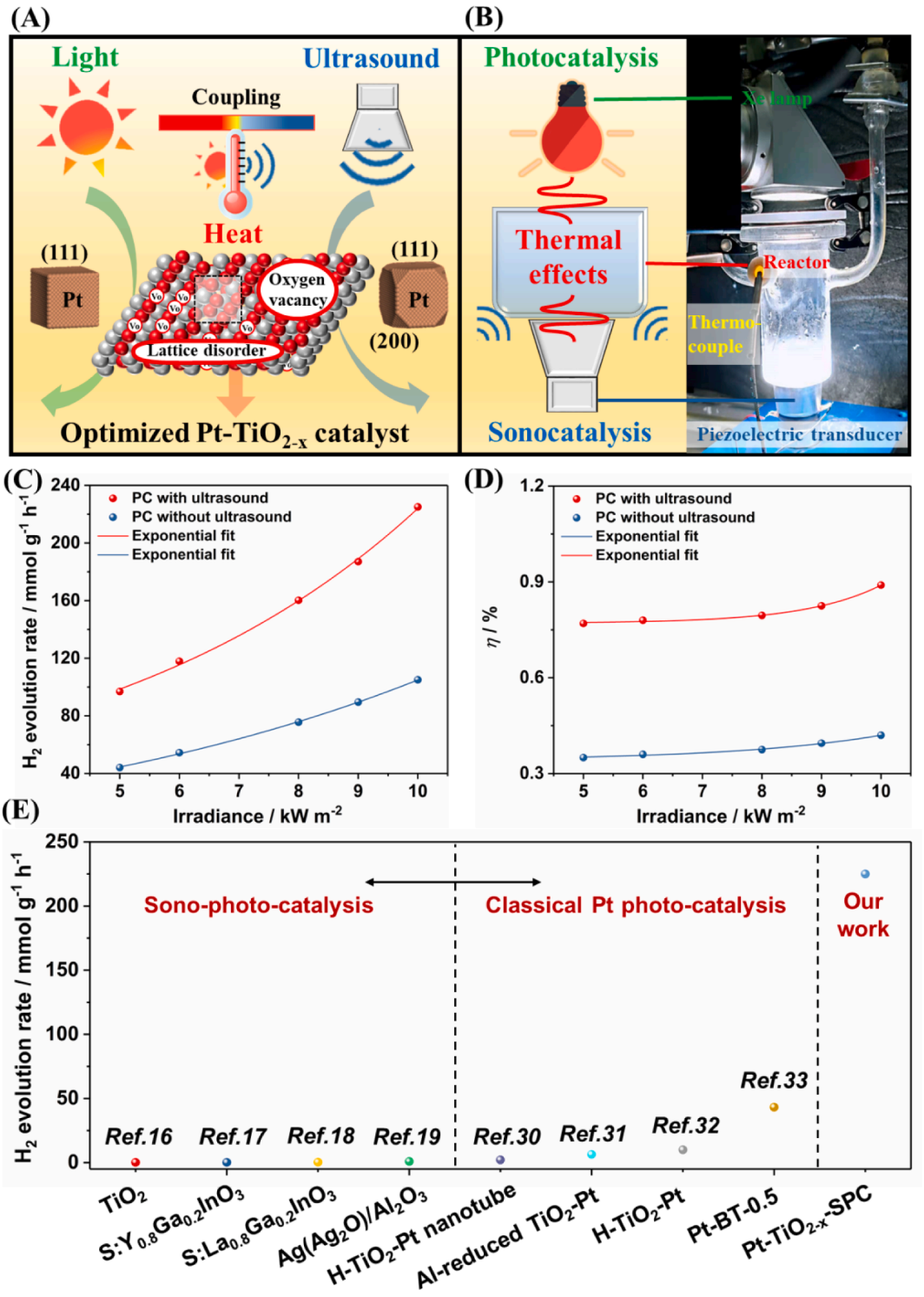

Fig. 1. (A) The schematic diagram of a sono-photo-thermo-coupled reaction system. (B) The photograph of a sono-photo-thermo-coupled reaction device. (C) PC hydrogen evolution rate against irradiance with and without ultrasound. (D) Solar-to-hydrogen efficiency against irradiance with and without ultrasound. (E) Hydrogen evolution rate over Pt-TiO_{2-x} catalysts in this work by contrast with the reported SPC systems and other similar Pt loaded TiO_2 photocatalysts.

by crossing activation energy barrier of redox reaction, promoting bond cleavage of water molecule and enhancing the amount of active radicals. On the other hand, acoustic streaming that derives from the attenuation of acoustic waves in fluids ameliorates the kinetic processes by promoting the dispersion of catalyst in reaction solutions [14], augmenting the mass transfer of reactive species to the catalyst surface and accelerating reactants adsorption/desorption [15]. However, very few studies have focused on SPC hydrogen evolution, leaving the fundamental mechanism still unclear. More importantly, although ultrasound has theoretically demonstrated the high feasibility to remarkably enhance the PC activity, the current performance (only ~μmol h^{-1} g^{-1}) [16–19] is yet far from the expectations.

In the scenario of SPC hydrogen evolution, the thermal effects are naturally coupled with the light and ultrasound. For the former, it is through the thermalization of unabsorbed photon and excited electrons [20], while for the latter, it is from the thermal dissipation of ultrasonic

mechanical energy and nebulization [15]. As a consequence, heat is intrinsic to any PC/SPC processes and cannot be technically decoupled. Meanwhile, it is more in line with the requirements of practical application for introducing thermal effects into PC/SPC systems. However, it has often been either ignored or intentionally eliminated by external cooling [21]. Besides huge losses and waste of the solar and acoustic energies, this may also be the main reason for failing to enhance significantly synergistic activity in SPC system, because heat is imperative for the hydrogen evolution as it is endothermic in nature and it has a crucial role in determining the thermodynamic and kinetic properties [21,22,25]. Note that there is conflicting conclusions in the study of thermal effects. Durán et al. has reported that high temperature is unfavorable to SPC reaction, because it could reduce the cavitation effects by decreasing the maximum temperature achieved upon bubble collapse and reducing the number of nuclei available for cavitation [26]. Therefore, it is necessary to implement a systematic and in-depth mechanistic study on the thermal effects in SPC system.

Herein, we firstly present a thermally-enhanced sono-photo-synergistic strategy that utilize the light- and ultrasonic-induced thermal effects to enhance the photo- and sono-catalytic hydrogen evolution activities simultaneously and dramatically improve the desired synergy of solar and acoustic energies, as illustrated in Fig. 1A and B. Our work, the best of our knowledge, delivers the highest record of hydrogen evolution rate (225.04 mmol g^{-1} h^{-1}) with the light-to-hydrogen efficiency of 0.89% compared to previous works in SPC reactions [16–19]. Besides, the present rate is 11 times of that in SPC without thermal effects. More impressively, thermal effects stimulate more effective synergy between light and ultrasound, achieving synergy enhancement index from 15% to 53%. This thermally-enhanced sono-photo-synergism mainly comes from the sono-photo-thermo-modulated structure optimization of Pt-TiO_2 catalyst to ameliorate catalytic properties in thermodynamic and kinetic processes. The lattice disordering of TiO_2 support with abundant point defects (Ti^{3+} and Vo) and the deaggregated Pt species with the coexistence of high-index (200) and low-index (111) facets are formed, which optimizes not only the thermodynamic properties by enhancing light harvesting and the charge redox power with sufficient driving force, but also the kinetic properties by accelerating the net charge separation and the whole processes of water splitting, including the dissociation of water molecules on high-index (200) Pt facets and production of H* intermediates on defect-rich TiO_{2-x} support and low-index (111) Pt facets. This study exemplifies that coupling light- and ultrasonic-induced thermal effects in SPC system could enhance the synergy between light and ultrasound by modulating catalyst structure to achieve double optimization of thermodynamic and kinetic properties of SPC hydrogen evolution.

2. Experimental section

2.1. Characterizations

X-ray photoelectron spectroscopy (XPS) measurements were carried out by the X-ray photoelectron spectrometer (ESCALAB Xi+, Thermo Fisher, USA). All binding energies were calibrated using the C 1 s peak at 284.6 eV. The Pt content of the sample was determined by inductively coupled plasma mass spectrometry (ICP-MS; NexION 350D, PerkinElmer, USA). Electron paramagnetic resonance (EPR) spectra of the samples were acquired by the X-band spectrometer (EMXplus A300–9.5/12/S-LC, Bruker, Germany). X-ray diffraction (XRD; LabX XRD-6100, SHIMADZU, Japan) measurements were used to characterize the crystal structures of the samples. The high-resolution transmission electron microscopy (HRTEM; JEM-2100, JEOL, Japan) images were acquired to characterize the morphologies of the samples. Ultraviolet-visible-near infrared diffuse reflectance spectra (UV–vis-NIR DRS) were taken using a UV-VIS-NIR spectrometer (Lambda 950, PerkinElmer, USA). The photoluminescence (PL) properties were investigated by fluorescence spectrophotometer (PE Lambda950, PerkinElmer, USA) with the excitation light at 270 nm.

2.2. Thermally-enhanced SPC experiments

The thermally-enhanced SPC hydrogen evolution was performed in a closed circulation system with top-radiation reactor. Pt species loaded defect-rich TiO_2 (Pt-TiO_{2-x}) catalyst was synthesized by facile *in-situ* sono-photo-thermo-treatment. 10 mg P25 TiO_2 (Macklin) and H_2PtCl_6 aqueous solution were suspended into 10 mL aqueous solution including 2 mL glycerol as sacrificial reagent due to its high boiling point and renewable properties from the by-product of biodiesel. The reaction system was completely degassed for about 30 min to completely remove air, followed by the SPC hydrogen evolution with a piezoelectric transducer as an acoustic source and a 300 W Xe lamp (CEL-PE300-3A, Beijing Teach Jinyuan Technology, China) with various irradiances as a light source, and no external heating and magnetic stirring instruments were applied. The piezoelectric transducer was located at the bottom of the reactor, and the ultrasonic power can be adjusted from 1 to 60 W by ultrasonic processor. The real-time temperature was monitored by K-type thermocouple connected to DAQ system. After ultrasonic and/or light irradiations, Pt nanoparticles were loaded on the surface of defects-rich TiO_{2-x} (Pt-TiO_{2-x}). Meanwhile, SPC hydrogen evolution was performed. The contents of hydrogen were quantified by an online gas chromatograph (GC9790II, Fuli Instruments, China) with a thermal conductive detector (TCD). An optimized Pt loading of 7.45 wt% has been verified based on the experimental results, and a schematic of the synthesis and reaction process for the Pt-TiO_{2-x} is shown in Fig. 1A and B.

The solar-to-hydrogen efficiency (η) was calculated by the following formula [14]:

$$\eta = \frac{\text{Output hydrogen energy}}{\text{Incident photon energy}} = \frac{\Delta G_{H_2} R_{H_2}}{I \times A} \times 100\%$$

where ΔG_{H_2} is the Gibbs free energy of formed H_2, ΔG_{H_2}= 237.20 kJ mol^{-1}; R_{H_2} is H_2 evolution rate, μmol h^{-1}; I is incident irradiance, kW m^{-2}; A is the incident area, A = 16.6 cm^2.

2.3. Photoelectrochemical measurements

The photoelectrochemical properties were performed on a PMC-1000/DC type electrochemical station (AMETEK) in a standard three-electrode system with 0.1 M Na_2SO_4 solution as the electrolyte. Pt electrode and Ag/AgCl (saturated KCl) electrode were used as the counter electrode and reference electrode respectively. AF-doped tin oxide (FTO) electrode deposited with Pt-TiO_{2-x} catalyst was used as work electrode.

2.4. DFT calculations

The first-principles calculations based on density functional theory (DFT) were performed by using the generalized gradient approximation (GGA) in the Perdew-Burke-Ernzerhof (PBE) form with the addition of the Hubbard term (DFT + U) [25,27]. All simulations were performed with the Quantum-Espresso code. The U value of titanium is 4.2 eV. The anatase TiO_2 (101) surface is chosen as the primary surface because it is the most exposed surface based on the XRD results. Convergence of the total energy, for bulk anatase, has been achieved using cutoffs of 40 and 480 Ry for wave functions and charge density respectively, and a grid of (4 × 4 × 2) *k*-points generated with the method of Monkhorst and Pack [28]. The (101) surface has been modeled with a rectangular (2 × 3) surface cell of size (10.4804 Å × 11.5601 Å), The TiO_2 slabs have a thickness of ~10 Å, and the vacuum between the TiO_2 slab and its copy is ~15 Å thick. All atomic positions were relaxed and atomic relaxations were performed until forces were smaller than 10^{-4} a.u. A p (4 × 4) supercell containing a 4-layer slab with 64 atoms was modeled for Pt

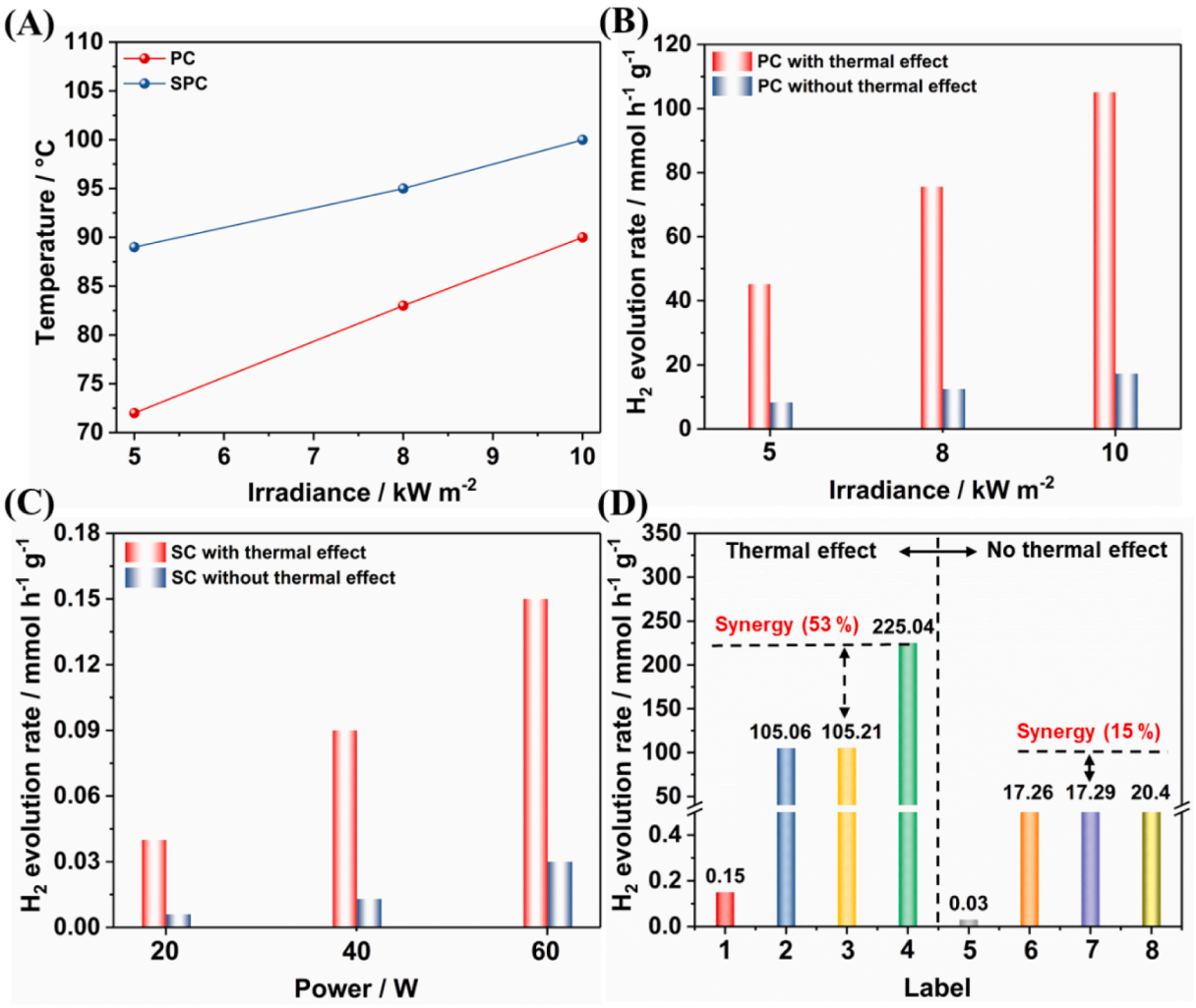

Fig. 2. (A) Solution temperature against irradiance under light irradiation assisted with and without ultrasound (28 kHz, 60 W). (B) PC hydrogen evolution rate under different irradiance with and without thermal effects. (C) SC hydrogen evolution rate under different ultrasonic power with and without thermal effects. (D) Hydrogen evolution rate under different conditions. Label 1 is under 28 kHz, 60 W ultrasonic irradiation, label 2 is under 10 kW m^{-2} irradiation, label 3 is sum of labels 2 and 3, Label 4 is under 10 kW m^{-2} irradiation assisted with ultrasound (28 kHz, 60 W), label 5 is under ultrasonic irradiation at 25 °C (cooling), label 6 is under 10 kW m^{-2} at 25 °C (cooling), label 7 is sum of labels 5 and 6, label 8 is under 10 kW m^{-2} assisted with ultrasound at 25 °C (cooling).

(200) and Pt (111) facets. Moreover, the free energies of hydrogen adsorption and water dissociation were calculated according to the following equation [27,29]:

$$\Delta G_{H^*} = \Delta E + \Delta E_{ZPE} - T\Delta S$$

where ΔE is the binding energy of hydrogen or water, ΔE_{ZPE} is the difference corresponding to the zero-point energy between the adsorbed atom and the gas phase, and $T\Delta S$ is the entropic contributions (T being 273.15 K).

3. Results and discussion

3.1. Performance of thermally-enhanced SPC hydrogen evolution

Preliminary investigations on the thermally-enhanced SPC hydrogen evolution efficiencies were carried out using *in-situ* formed Pt-TiO_{2-x} as catalyst. Fig. 1C and D illustrate the H_2 evolution rate (RH_2) and the solar-to-hydrogen efficiency (η) under different irradiances of 5, 8 and 10 kW m^{-2}. Interestingly, the RH_2 and η are exponentially correlated to the irradiance by data-fitting, which differs from the normally linear correlation in traditional photon-driven reaction [21], showing the attractive advantage of hydrogen evolution by increasing irradiance. The exponentially enhanced hydrogen evolution against irradiance can be mainly attributed to the uni-source photo-thermal synergism with the enhancement of ultrasound, which is the coupling of thermally-optimized photocatalyst structure and thermally-enhanced SPC water splitting [21–24]. For all cases, both RH_2 and η with ultrasonic irradiation are all higher than those without ultrasonic irradiation. The maximum RH_2 of 225.04 mmol g^{-1} h^{-1} and η of 0.89% are obtained under 10 kW m^{-2} irradiation with ultrasound (28 kHz at 60 W), while the significantly decreased RH_2 (105.06 mmol g^{-1} h^{-1}) and η (0.42%) are observed under the identical conditions without ultrasound, thereby ultrasound effects contribute to 53.31% enhancement of SPC hydrogen evolution, demonstrating the significant impact.

of ultrasonic irradiation on the enhanced PC hydrogen evolution. To the best of our knowledge, the present RH_2, is far more efficient than any previously reported SPC systems (Fig. 1E, Table S1) [16–19], and is also higher than the most performances of similar Pt loaded TiO_2 [30–33]. Additionally, the cycling hydrogen evolution under 10 kW m^{-2} irradiation assisted with ultrasound (28 kHz, 60 W) is tested. As shown in Fig. S1, no noticeable hydrogen evolution rate decreasing is observed after five runs, indicating a good reproducibility of high-efficient SPC hydrogen evolution.

To shed light on the origin of remarkable enhancement of SPC

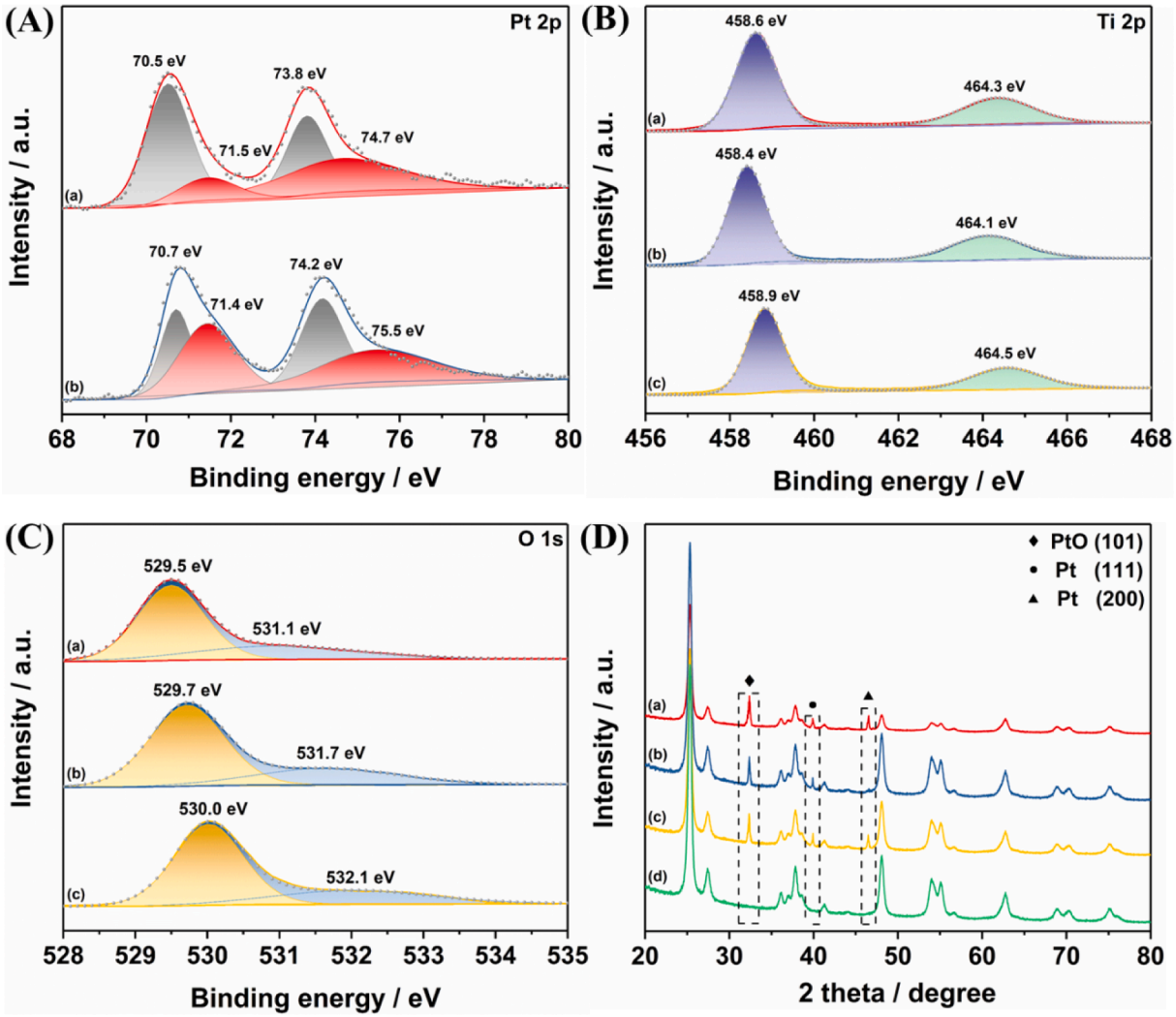

Fig. 3. (A) Pt 4f XPS spectra of (a) Pt-TiO_{2-x}-SPC and (b) Pt-TiO_{2-x}-PC; (B) Ti 2p and (C) O 1 s XPS spectra of (a) Pt-TiO_{2-x}-SPC, (b) Pt-TiO_{2-x}-PC and (c) TiO_2; (D) XRD patterns of (a) Pt-TiO_{2-x}-SPC, (b) Pt-TiO_{2-x}-PC, (c) Pt-TiO_{2-x}-SC and (d) TiO_2.

hydrogen evolution performances in our reaction system, a series of comparative experiments were conducted. In the sole PC hydrogen evolution with full-spectrum irradiation, the solution temperature with the irradiances of 5, 8 and 10 kW m^{-2} spontaneously increases and finally remains at 72, 83 and 90 °C, respectively (Fig. 2A), indicating the light-induced thermal effect that is the consequence of the thermalization of unabsorbed photon and excited electrons. As shown in Fig. 2B, the RH_2 under 5, 8 and 10 kW m^{-2} irradiation are 45.21, 75.58 and 105.06 mmol g^{-1} h^{-1} respectively, while the RH_2 without thermal effect by thermostat cooling are significantly decreased to 8.33, 12.44 and 17.26 mmol g^{-1} h^{-1} respectively. The obvious thermally-enhanced effect on PC hydrogen evolution can be a collective effect of multistage processes, mainly including thermodynamic optimization of the decreasing apparent activation energy and the increasing the formation of hot electron and reactant molecules in excited states, and kinetic modulation of promoting diffusion of reactants, the mobility and transfer of photo-generated charge carriers and the rate of adsorption-desorption, which have been confirmed by previous reports [20–22]. In the sole sonocatalytic (SC, 28 kHz) hydrogen evolution, the solution temperature increases from 35 to 44 °C with the increase of ultrasonic powers from 20 to 60 W (Fig. S2), suggesting the inherent ultrasonic-induced thermal effect as a consequence of the thermal dissipation of ultrasonic mechanical energy and nebulization [15]. It can be found that ultrasound could directly trigger water to be cracked to generate obvious hydrogen (0.15 mmol g^{-1} h^{-1}) at 60 W, while only a bit of hydrogen (0.03 mmol g^{-1} h^{-1}) is detected when the thermal effect is removed by thermostat cooling (Fig. 2C), thereby the ultrasonic-induced thermal effect is kinetically beneficial for H_2O activation to decompose into active hydrogen atoms and subsequently promoted the SC activity.

In the comprehensive SPC hydrogen evolution, the solution temperature further increases when ultrasound (28 kHz, 60 W) is introduced into PC system, 89, 99 and 103 °C are obtained with the irradiances of 5, 8 and 10 kW m^{-2} respectively (Fig. 2A). Under 10 kW m^{-2} irradiation assisted with ultrasound (28 kHz, 60 W), the RH_2 plummets by an order of magnitude from 225.04 to 20.4 mmol g^{-1} h^{-1} when the coupling light- and ultrasonic-induced thermal effects are removed by thermostat cooling, confirming that the thermal effects play a decisive role in significantly enhanced SPC activity. Moreover, the RH_2 of thermally-enhanced SPC system is higher than the sum of those under sole light and ultrasonic irradiation with thermal effects, thereby there is a synergism driven by these external multi-fields coupling. In order to further quantify the participation of ultrasound in PC system, the synergy index (SI) is calculated by the following formula [13,34]:

$$\text{Synergy index } (\%) = \frac{R_{SPC} - (R_{PC} + R_{SC})}{R_{SPC}}$$

where R_{SPC}, R_{PC}, and R_{SC} are sono-photo-, photo- and sono-catalytic hydrogen rates respectively. More impressively, the synergy index of

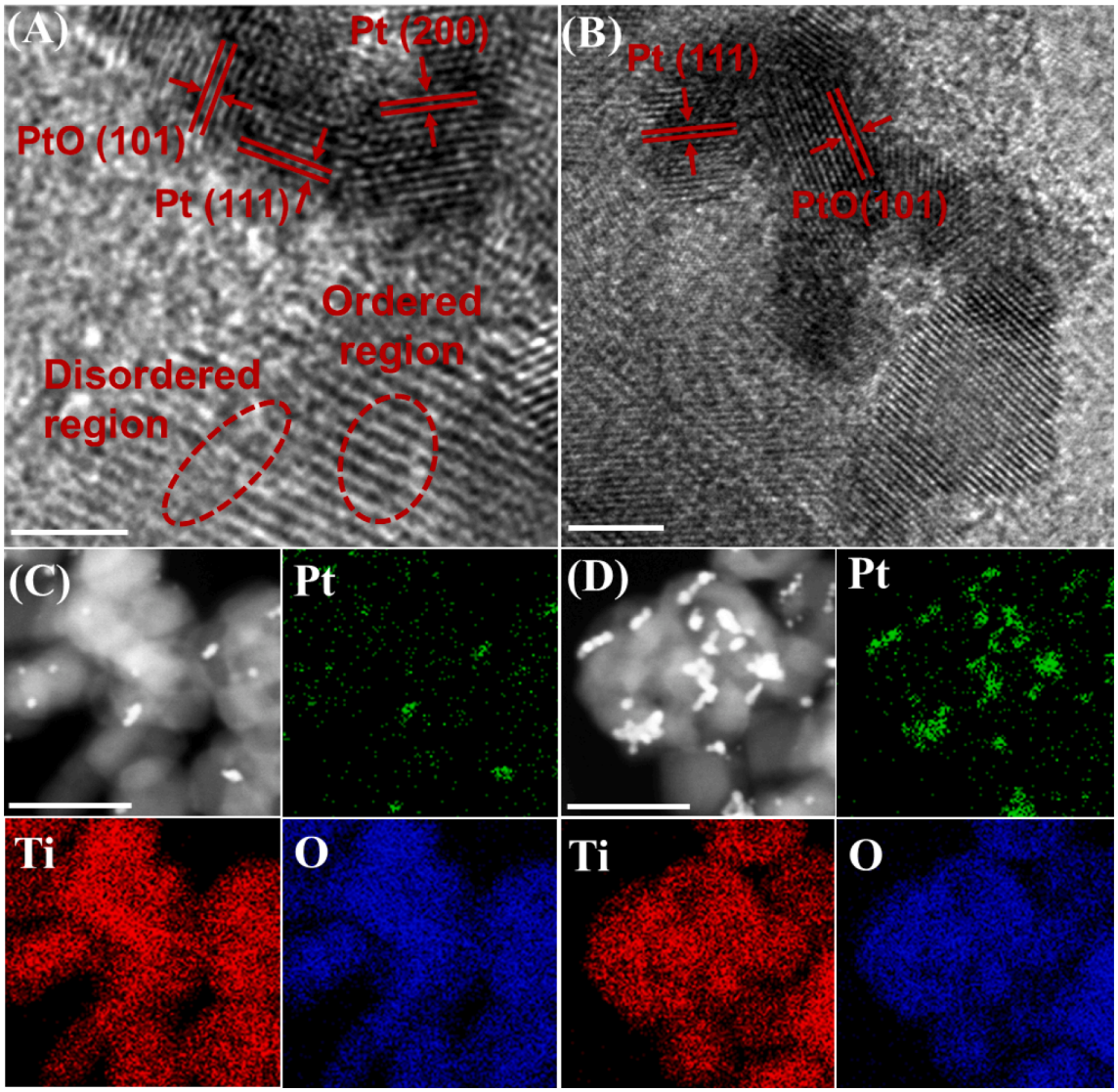

Fig. 4. HRTEM images of (A) Pt-TiO_{2-x}-SPC and (B) Pt-TiO_{2-x}-PC (scale: 5 nm; HAADF-STEM images and the corresponding EDX elemental mapping images for (C) Pt-TiO_{2-x}-SPC and (D) Pt-TiO_{2-x}-PC (Scale: 50 nm).

SPC without thermal effects is only 15%, while there is increased to 53% with thermal effects, manifesting that light- and ultrasonic-induced thermal effects could reshape the growth of SPC activity by stimulating a higher degree of synergy.

3.2. Geometrically structural optimization of Pt-TiO_{2-x} catalysts

In order to deeply understand the structure-performance relationship at atomic level under this novel thermally-enhanced SPC system, the physicochemical properties of the *in-situ* formed Pt-TiO_{2-x} catalyst were investigated. The X-ray photoelectron spectroscopy (XPS) elemental survey scan shows that Pt-TiO_{2-x}-SPC includes Pt, Ti and O elements (Fig. S3). As shown in Fig. 3A, the Pt 4f XPS peaks of Pt-TiO_{2-x}-SPC at 70.5 eV and 73.8 eV are corresponding to Pt^0 $4f_{7/2}$ and Pt^0 $4f_{5/2}$ respectively [25], and the peaks at 71.5 eV and 74.7 eV are assigned to Pt^{2+} $4f_{7/2}$ and Pt^{2+} $4f_{5/2}$, respectively [35]. The binding energies of Pt 4f in Pt-TiO_{2-x}-SPC are negatively shifted compared with Pt-TiO_{2-x}-PC, implying that the introduction of ultrasound into the PC process could increase electron density of Pt species by charge transfer from TiO_2 to Pt. Moreover, the proportions of Pt^0 and Pt^{2+} in Pt-TiO_{2-x}-PC/Pt-TiO_{2-x}-SPC are 76.43/80.91% and 13.57/19.09% respectively. A higher proportion of Pt^0 in Pt-TiO_{2-x}-SPC further confirms ultrasonic-induced more electron density of Pt species, this increased electron density in similar systems can be considered as the source of enhanced catalytic activity by strong metal-support interaction [25,36]. Note that, compared with original TiO_2, the Ti 2p and O 1 s peaks in Pt-TiO_{2-x}-PC and Pt-TiO_{2-x}-SPC shift toward lower binding energy (Fig. 3B and C), implying the formation of low-charge Ti ions and oxygen vacancies (Vo) under the action of the ultrasonic and light irradiations. To further verify the defect-rich nature of Pt-TiO_{2-x} catalyst, the electron spin resonance (EPR) analysis has been conducted (Fig. S4). No obvious signal is observed in original TiO_2, while stronger signals of the paramagnetic Ti^{3+} centers (g = 1.942, 1.981) and Vo (g = 2.003) appear in Pt-TiO_{2-x}-SPC than that in Pt-TiO_{2-x}-PC [21], showing structural defects can be adjusted efficiently through the introduction of ultrasonic field into PC system. Combining the increased superoxide radical O_2^- at g = 2.035 that derives from the electron transfer from the catalyst surface to adsorbed oxygen [21,37], it is demonstrated that the defect-rich nature is beneficial for the separation of photo-generated electron and hole pairs.

The crystal structure of the synthesized catalysts was investigated by X-ray powder diffraction (XRD) patterns. As displayed in Fig. 3D, the related peaks of TiO_2 anatase and rutile phases are clearly seen in all the samples, while there is significantly different peak intensities in the

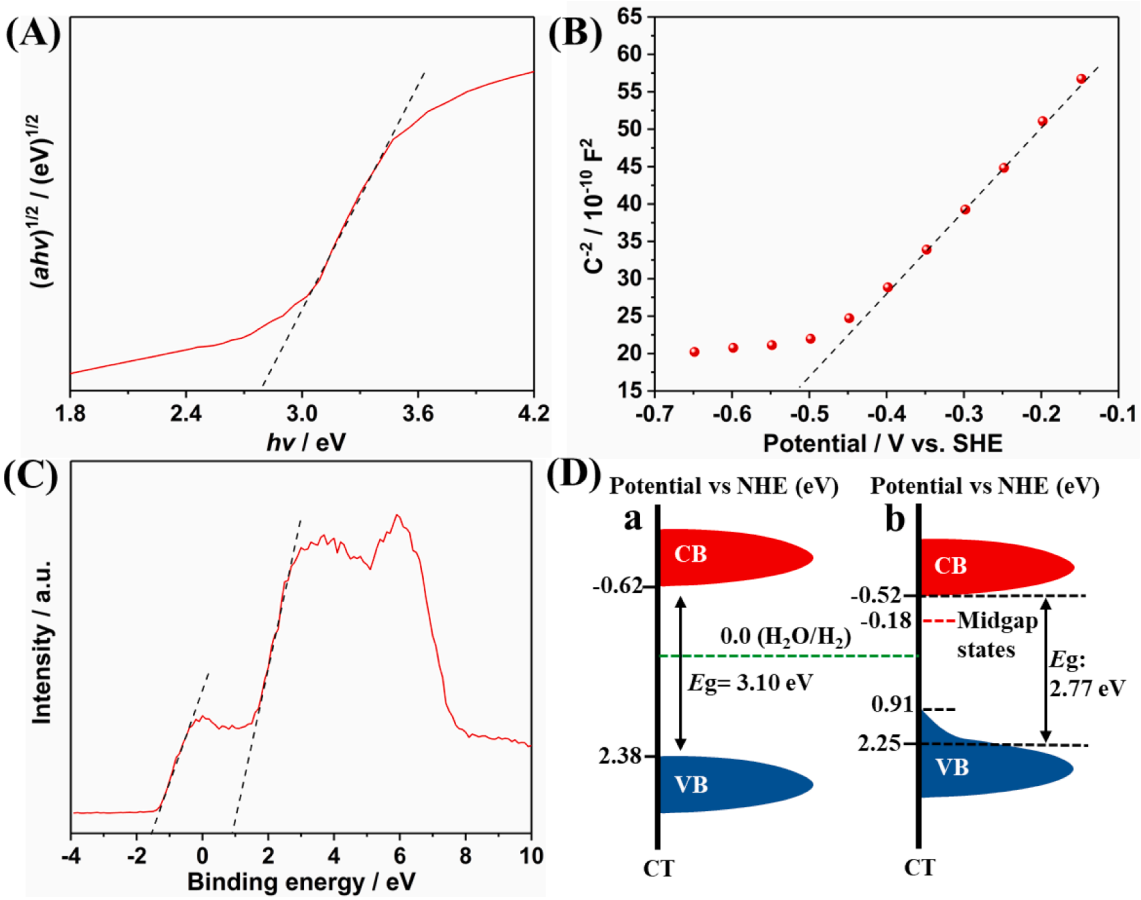

Fig. 5. (A) Tauc plot, (B) Mott-Schottky plot and (C) VB XPS spectrum of Pt-TiO_{2-x}-SPC. (D) Band energy diagram of (a) TiO_2 and (b) Pt-TiO_{2-x}-SPC.

order of original TiO_2 ≈ Pt-TiO_{2-x}-PC > Pt-TiO_{2-x}-US > Pt-TiO_{2-x}-SPC, suggesting the formation of lattice-disordered TiO_2 support as the result of the disruption of perfect periodic arrangement of atoms [38]. Note that the ultrasound serves as the main impetus to reduce the distortion energy of TiO_2 with disorder structure due to nearly no change in crystalline structure when sole light irradiation is applied, but the light irradiation could collaboratively enhance ultrasonic-induced disorder engineering. Besides the characteristic peaks of TiO_2 in all samples, the low-index crystalline Pt species appear in the form of PtO (101) and metallic Pt (111) at $2\theta = 32.4^\circ$ (JCPDS, 47–1171) and 39.9° (JCPDS, 04–0802) respectively [39]. More impressively, high-index Pt (200) facet at $2\theta = 46.5^\circ$ (JCPDS, 04–0802) is only observed in Pt-TiO_{2-x}-US and Pt-TiO_{2-x}-SPC, but not in Pt-TiO_{2-x}-PC. Such high-index facets, denoted by a set of Miller indices {hkl} with at least one index greater than unity [40], generally show much higher catalytic activity than that of the low-index facets due to its high density of atomic steps, ledges and kinks as active sites for breaking chemical bonds [41]. Unlike the thermodynamically more stable of low-index facets, however, it is rather challenging in synthesis owing to the thermodynamic limitation of the high-index facets with high surface energy tended to disappear during particle formation. Toward this end, above results reveal that integrating ultrasound into PC system could break the thermodynamic limitation of high-index facets formation, which is promising favorable for the enhanced solar to hydrogen evolution efficiency.

The high-resolution transmission electron microscope (HRTEM) images of Pt-TiO_{2-x}-PC and Pt-TiO_{2-x}-SPC exhibit that, unlike the well-resolved anatase and rutile fringes of original TiO_2 (Fig. S5), the coexistence of "two phases": ordered regions with distinct lattice fringes and disordered regions with distorted crystal lattice can be clearly observed (Fig. 4A and B). Furthermore, the detailed microstructure of Pt species is manifested in Fig. 4A and B. The lattice spacing of 0.272 nm corresponding to PtO (101) is discerned in Pt-TiO_{2-x}-PC and Pt-TiO_{2-x}-SPC. The lattice fringes with distances of 0.229 and 0.198 nm are clearly observed in the Pt-TiO_{2-x}-SPC and are attributed to the metallic Pt (111) and (200) planes respectively [35], while there is only metallic Pt (111) plane in Pt-TiO_{2-x}-PC, it is coincided well with the XRD results. Such different crystal facets of Pt species will drive directionally the separation of photo-generated charges in space. The Pt species in Pt-TiO_{2-x}-SPC with an particle size of 2–5 nm are well-dispersed on the defects-rich TiO_{2-x} support (Fig. 4C), while the aggregated Pt nanoparticles with average size of 10 nm are readily visualized in Pt-TiO_{2-x}-PC (Fig. 4D), indicating ultrasonic-induced the deaggregation of Pt species to allow more active sites to be available for reactants. Note that the atomic vacancy defect is found within the Pt crystal facets (Fig. 4A), which could induce the unsaturated coordination of Pt species and enable enhanced catalytic activities [42].

3.3. *Thermodynamically tunable light harvesting and redox potential*

In view of the optimized morphological structure in Pt-TiO_{2-x}-SPC, thermodynamic modulation of light harvesting and suitable redox potential with sufficient driving force is expected. Compared with original TiO_2 and Pt-TiO_{2-x}-PC, the Pt-TiO_{2-x}-SPC exhibits extended and intensive light absorption in visible and NIR regions (Fig. S6), which can be ascribed to the emergence of additional electronic states from the lattice disorder and point defects (Ti^{3+} and Vo) in the TiO_2 support and the atomic vacancy in deaggregated Pt species. To shed light on the formation of midgap electronic states, the band structure of Pt-TiO_{2-x}-SPC is studied. Narrowed bandgap from 3.10 eV of TiO_2 to 2.77 eV of Pt-TiO_{2-x}-SPC is calculated by Kubelka-Munk method (Fig. 5A and Fig. S7). The

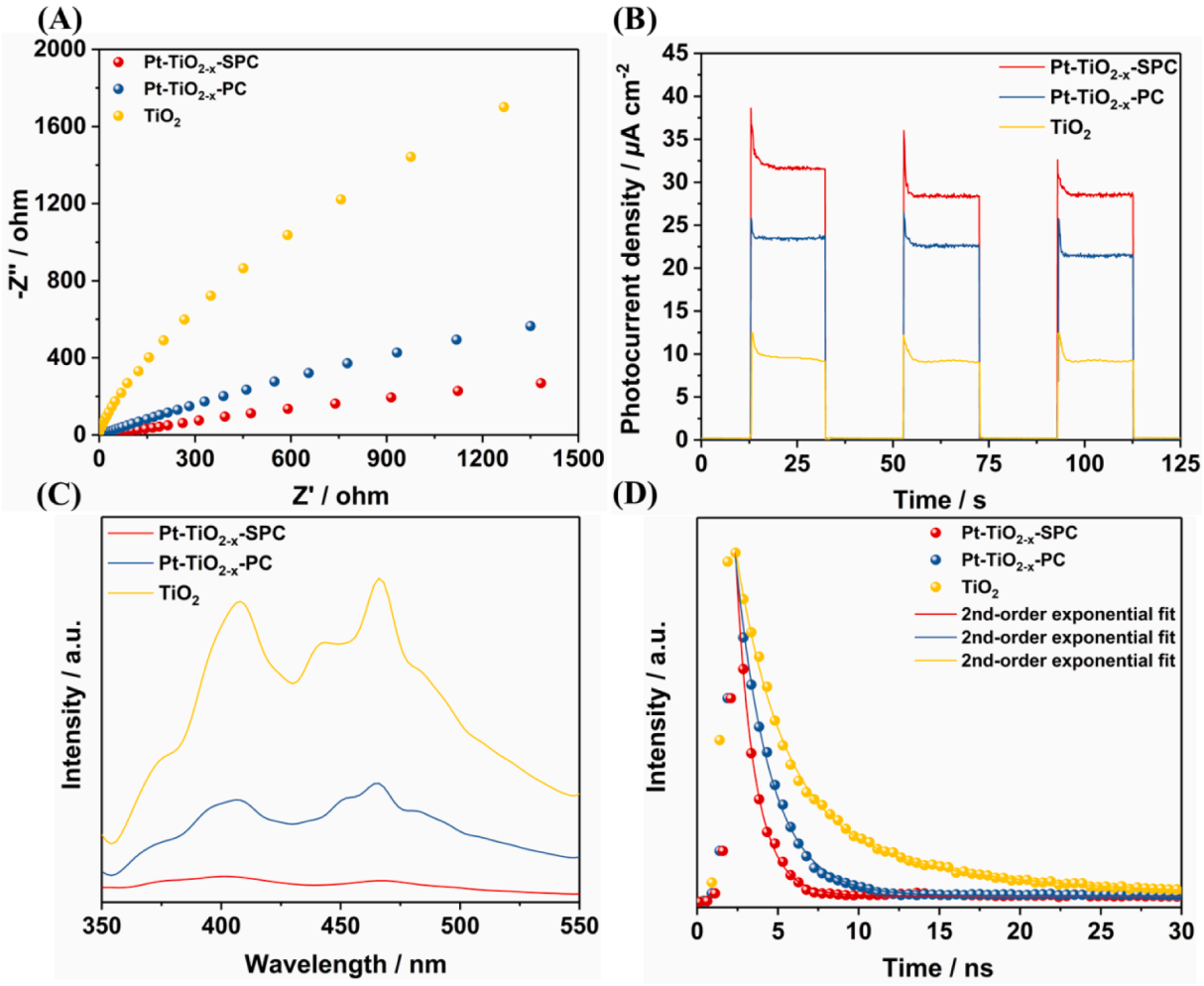

Fig. 6. (A) EIS Nyquist plots, (B) Transient photocurrent responses, (C) Photoluminescence (PL) and (D) Transient PL decay spectra of Pt-TiO_{2-x}-SPC, Pt-TiO_{2-x}-PC and TiO_2.

corresponding potential of conduction band (CB) edge that is approximately equals to the flat-band potential is −0.52 eV by the Mott-Schottky analysis (Fig. 5B) [21,43], thereby the valence band (VB) edge of Pt-TiO_{2-x}-SPC is evaluated to be at 2.25 eV. As shown in Fig. 5C, the VB XPS spectra illustrate the main absorption onset at 0.91 eV, as well as a significant blueshift of VB maximum energy related with the band tail to −1.52 eV, demonstrating the existence of midgap electronic states between the VB and CB of Pt-TiO_{2-x}-SPC and the potential is evaluated to be −0.18 eV (=[2.25 - (0.91 - (− 1.52) eV) [43]. Such potential value meets the redox potential of hydrogen proton reduction to directly extend the pathway of hydrogen evolution, and the band structure is schematically illustrated in Fig. 5D.

3.4. Kinetically adjustable charge separation and reactant adsorption-desorption

In general, the photo-excited charge separation and reactant adsorption-desorption are crucial factors for affecting kinetic properties of the reaction. To unveil the kinetics of thermally-enhanced SPC reaction, the charge separation efficiency is firstly investigated. Compared with original TiO_2, Pt-TiO_{2-x}-SPC shows smaller the diameter of the Nyquist circle (Fig. 6A), higher transient photocurrent response (Fig. 6B), lower PL emission intensity (Fig. 6C) and shorter average emission lifetime (Fig. 6D, Table S2), which cooperatively verify reduced interfacial charge transfer resistance, suppressed charge recombination and accelerated consumption and separation of charge carriers [3,4]. Such complementary electro- and photo-chemical tests manifest the ultrasonic-intensified dynamics. This optimized charge separation dynamics are attributed to not only the introduction of additional electronic states to broaden the charge transfer channel, but also the formation of heterojunction of PtO and TiO_{2-x} and Schottky barrier of metallic Pt and TiO_{2-x}. The unique Pt^{2+}/Pt^0 couples are also favorable for the charge separation on different sites where Pt^{2+} traps electron and Pt^0 traps hole. Note that the charge separation in Pt-TiO_{2-x}-SPC is more efficient than that in Pt-TiO_{2-x}-PC (Fig. 6A~D), which results from the smaller size and different crystal facets of Pt (111) and Pt (200) through shortening transfer distance and directionally spatial separation of charge [12], respectively.

Secondly, DFT calculations were performed to in-depth elucidate the reactant adsorption and product desorption behaviors. The whole hydrogen evolution pathway is typically treated as a combination of three elementary steps [27,44]: (1) Initial hydrogen proton (H^+) generation by water adsorption and subsequent dissociation; (2) Intermediate H* formation ($H^+ + e^- + * \rightarrow H^*$, where * refers to catalyst surface); (3) Final H_2 evolution by the combination of H*. The Gibbs free-energy of H adsorption (ΔG_{H^*}) on the catalyst has been generally used to estimate its hydrogen evolution activity, and highly efficient hydrogen evolution catalyst has a ΔG_{H^*} close to zero that implies a faster charge transfer for both H* intermediate and H_2 evolution [44]. The theoretical models of Pt loaded TiO_2 catalysts with/without Vo are shown in Fig. S8. The ΔG_{H^*} values of Pt nanoparticles on defective TiO_{2-x} and stoichiometric TiO_2 are −0.54 eV and − 0.78 eV respectively

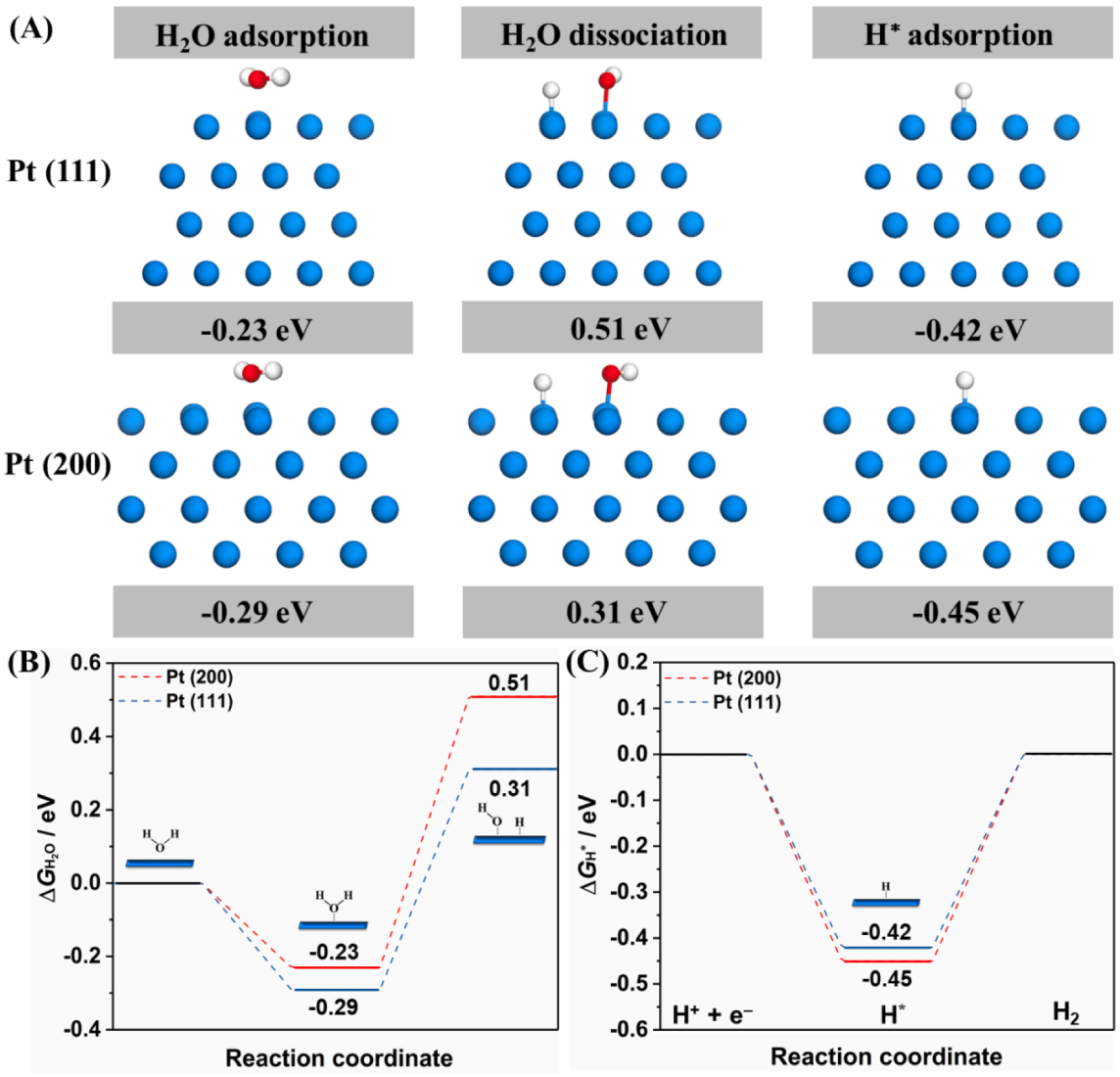

Fig. 7. (A) The most stable adsorption configurations of the key intermediates of hydrogen evolution on Pt (200) and (111) facets (the white, red and blue spheres represent O, H and Pt atoms, respectively). The energy profiles along the reaction coordinates for (B) water absorption and dissociation, and (C) hydrogen evolution.

(Fig. S9), thereby there is a favorable H* adsorption-desorption property for defect-rich Pt-TiO_{2-x}.

Additionally, to further synthetically understand how the different Pt facets work to facilitate the whole hydrogen evolution process, the water adsorption-dissociation and H* absorption behaviors on both low-index Pt (111) and high-index Pt (200) facets are investigated, as shown in Fig. 7A. The adsorption energy of water on Pt (200) facet (−0.29 eV) is more negative than that on Pt (111) facet (−0.23 eV) (Fig. 7B), indicating that water is preferentially adsorbed on Pt (200) facet [45]. Moreover, the activation barrier of water dissociation (ΔG_{H2O}) on Pt (200) facet (0.31 eV) is lower than that on Pt (111) facet (0.51 eV) (Fig. 7B), suggesting more favorable water dissociation on Pt (200) facet than that on Pt (111) facet [36]. In conjunction with optimal water absorption on Pt (200) facet, the whole activation processes of water molecules are facilitated on high-index Pt (200) facet compared with low-index Pt (111) facet. While the ΔG_{H^*} of Pt (111) and Pt (200) facets are −0.42 eV and − 0.45 eV respectively (Fig. 7C), thereby a faster combination of intermediate H* on low-index Pt (111) to form molecular H_2. The joint collaboration of high-index Pt (200) facet with promoted water adsorption-dissociation and low-index Pt (111) facet with favorable H* absorption behavior affords Pt species of Pt-TiO_{2-x}-SPC superior hydrogen evolution.

3.5. Synergism of thermally-enhanced SPC hydrogen evolution

Based in all the above experimental and calculation results, the novel synergism of thermally-enhanced SPC hydrogen evolution is summarized and proposed in terms of thermodynamics and kinetics as follows (Fig. 8):

(1) Under the combined conditions of ultrasonic and light accompanied with thermal effects, the Pt loaded TiO_2 catalysts exhibit positive response in terms of the collaborative modulations of the morphological and electronic characteristics. Specifically, the lattice disordering of TiO_2 support with abundant point defects (Ti^{3+} and Vo) and the deaggregated Pt species with the coexistence of high-index (200) and low-index (111) facets appear.

(2) Such optimized morphology and electronic structure could narrow the bandgap and reshape the redox potential of charge by regulating CB states and create additional defects states, which, from the view of thermodynamics, is beneficial for extending the light absorption in visible and infrared regions and strengthening the driving force for hydrogen proton reduction.

(3) The charge separation and reactant adsorption-desorption dynamics are further facilitated due to the above-mentioned sono-

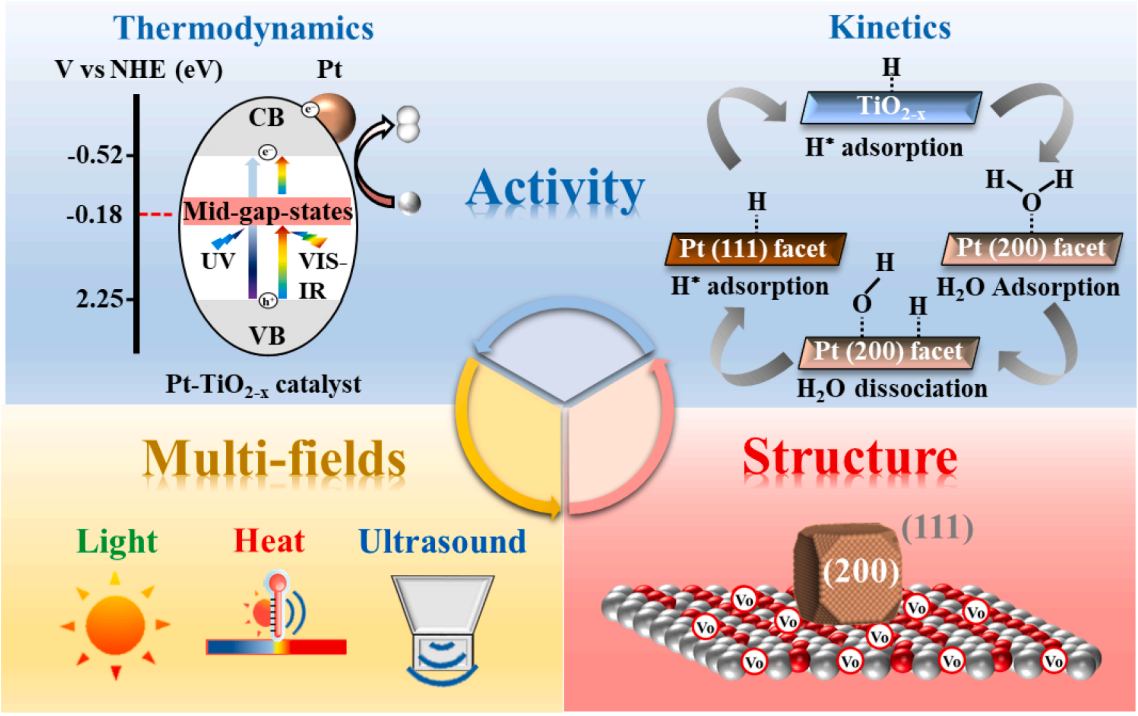

Fig. 8. Schematic presentation of the proposed synergism of thermally-enhanced SPC hydrogen evolution.

photo-thermo-induced catalyst optimization. On the one hand, the migration paths are shortened and widened simultaneously, which, from the view of kinetics, increases the net efficiency of charge separation. On the other hand, a faster dissociation of water molecules on high-index (200) Pt facets and a more efficient production of H* intermediates on defect-rich TiO_{2-x} support and low-index (111) Pt facets are achieved, thereby leading to a remarkably thermally-enhanced SPC performance.

4. Conclusions

Since the thermal effect is intrinsically coupled with ultrasound and light, we find it a highly potential and convenient candidate to improve the performance of SPC once the multi-field stimuli are harmonically synergized. In the present work, we systematically investigate and convincingly demonstrate that the intrinsic thermal enhancement in SPC is essentially a higher-degree synergy between thermally-enhanced SC and PC. By appropriately manipulation, a high-efficient hydrogen evolution rate of 225.04 mmol g^{-1} h^{-1} with light-to-hydrogen efficiency of 0.89% has been achieved in thermally-enhanced SPC, confirming a synergy index up to 53%. We found that this thermally-enhanced sono-photo-synergism mainly comes from the sono-photo-thermo-modulated structure optimization of Pt-TiO_{2-x} catalyst to ameliorate the catalytic properties in terms of thermodynamics and kinetics. Theoretical calculations and experimental results verify the existence of defect-rich TiO_2 support and deaggregated Pt species with functional complementary lattice facets, which not only ameliorates the light harvesting and the charge redox potential, but also accelerates the net efficiency of charge separation and the whole processes of water splitting, including the dissociation of water molecules on high-index (200) Pt facets and production of H* intermediates on defect-rich TiO_{2-x} support and low-index (111) Pt facets. This study exemplifies that utilizing intrinsic thermal effects in SPC can enhance the synergy between light and ultrasound and optimize the reaction thermodynamic and kinetic properties for achieving high-efficient SPC hydrogen evolution.

Credit authorship contribution statement

Rong Ma: Conceptualization, Data curationm Formal analysis, Investigation, Writing – original draft, Writing – review & editing. **Hui Su:** Software, Methodology. **Jie Sun:** Funding acquisition, Project administration, Resources, Supervision, Validation. **Donghui Li:** Supervision. **Zhenwen Zhang:** Supervision. **Jinjia Wei:** Supervision.

Declaration of Competing Interest

The authors declare that they have no known competing financial interests or personal relationships that could have appeared to influence the work reported in this paper.

Data availability

No data was used for the research described in the article.

Acknowledgments

This work is financially supported by the National Natural Science Foundation of China (52176202) and the Foshan Xianhu Laboratory of the Advanced Energy Science and Technology Guangdong Laboratory (41200101).

Appendix A. Supplementary data

Supplementary data to this article can be found online at https://doi.org/10.1016/j.ultsonch.2022.106222.

References

[1] N.S. Lewis, Research opportunities to advance solar energy utilization, Science 351 (2016) 1920–1928.
[2] H. Nishiyama, T. Yamada, M. Nakabayashi, Y. Maehara, M. Yamaguchi, Y. Kuromiya, Y. Nagatsuma, H. Tokudome, S. Akiyama, T. Watanabe, R. Narushima, S. Okunaka, N. Shibata, T. Takata, T. Hisatomi, K. Domen, Photocatalytic solar hydrogen production from water on a 100-m^2 scale, Nature 598 (2021) 304–312.

[3] Z. Wang, C. Li, K. Domen, Recent developments in heterogeneous photocatalysts for solar-driven overall water splitting, Chem. Soc. Rev. 48 (2019) 2109–2125.

[4] Y. Tang, W. Zhou, Q.Q. Shang, Y.C. Guo, H.L. Hu, Z.Q. Li, Y.Z. Zhang, L.Q. Liu, H. Y. Wang, X. Tan, T. Yu, J.H. Ye, Discerning the mechanism of expedited interfacial electron transformation boosting photocatalytic hydrogen evolution by metallic 1T-WS_2-induced photothermal effect, Appl. Catal. B Environ. 310 (2022) 121295–121304.

[5] Y. Li, H. Chang, Z.F. Wang, Q.Q. Shen, X.G. Liu, J.B. Xue, H.S. Jia, A 3D C@TiO_2 multishell nanoframe for simultaneous photothermal catalytic hydrogen generation and organic pollutant degradation, Colloid Interf. Sci. 609 (2022) 535–546.

[6] Y. Li, J.B. Xue, Q.Q. Shen, S.F. Jia, Q. Li, Y.X. Li, X.G. Liu, H.S. Jia, Construction of a ternary spatial junction in yolk-shell nanoreactor for efficient photo-thermal catalytic hydrogen generation, Chem. Eng. J. 423 (2021), 130188–13102.

[7] Q.Q. Shen, J.B. Xue, Y. Li, G.X. Gao, Q. Li, X.G. Liu, H.S. Jia, B.S. Xu, Y.C. Wu, S. J. Dillon, Construction of CdSe polymorphic junctions with coherent interface for enhanced photoelectrocatalytic hydrogen generation, Appl. Catal. B Environ. 282 (2021) 119552–119562.

[8] B. Ohtani, Revisiting the fundamental physical chemistry in heterogeneous photocatalysis: its thermodynamics and kinetics, Phys.Chem.Chem.Phys. 16 (2014) 1788–1797.

[9] J.W. Fu, K.X. Jiang, X.Q. Qiu, J.G. Yu, M. Liu, Product selectivity of photocatalytic CO_2 reduction reactions, Mater. Today 32 (2020) 222–243.

[10] J.Q. Gao, J.B. Xue, Q.Q. Shen, T.W. Liu, X.C. Zhang, X.G. Liu, H.S. Jia, Q. Li, Y. C. Wu, A promoted photocatalysis system trade-off between thermodynamic and kinetic via hierarchical distribution dual-defects for efficient H_2 evolution, Chem. Eng. J. 431 (2022) 133281–133293.

[11] B.S. Liu, X.J. Zhao, C. Terashima, A. Fujishimab, K. Nakata, Thermodynamic and kinetic analysis of heterogeneous photocatalysis for semiconductor systems, Phys. Chem.Chem.Phys. 16 (2014) 8751–8760.

[12] C. Hu, S.C. Tu, N. Tian, T.Y. Ma, Y.H. Zhang, H.W. Huang, Photocatalysis enhanced by external fields, Angew. Chem. Int. Ed. 60 (2021) 16309–16328.

[13] S.G. Anju, S. Yesodharan, E.P. Yesodharan, Zinc oxide mediated sonophotocatalytic degradation of phenol in water, Chem. Eng. J. 189-190 (2012) 84–93.

[14] V. Frenkel, R. Gurka, A. Liberzon, U. Shavit, E. Kimmel, Preliminary investigations of ultrasound induced acoustic streaming using particle image velocimetry, Ultrason. Sonochem. 39 (2001) 153–156.

[15] M.H. Islam, O.S. Burheim, B.G. Pollet, Sonochemical and sonoelectrochemical production of hydrogen, Ultrason. Sonochem. 51 (2019) 533–555.

[16] H. Harada, Sonophotocatalytic decomposition of water using TiO_2 photocatalyst, Ultrason. Sonochem. 8 (2001) 55–58.

[17] M. Penconi, F. Rossi, F. Ortica, F. Elisei, P.L. Gentili, Hydrogen production from water by photolysis, sonolysis and sonophotolysis with solid solutions of rare earth, gallium and indium oxides as heterogeneous catalysts, Sustainability 7 (2015) 9310–9325.

[18] P.L. Gentili, M. Penconi, F. Ortica, F. Cotana, F. Rossi, F. Elisei, Synergistic effects in hydrogen production through water sonophotolysis catalyzed by new $La_{2x}Ga_{2y}In_{2(1-x-y)}O_3$ solid solutions, Int. J. Hydrog. Energy 34 (2009) 9042–9049.

[19] R.D. Senevirathne, L.K. Abeykoon, N.L. Silva, C.F. Yan, J. Bandara, Sono-photocatalytic production of hydrogen by interface modified metal oxide insulators, Ultrason. Sonochem. 45 (2018) 279–285.

[20] M.Q. Yang, M.M. Gao, M.H. Hong, G.W. Ho, Visible-to-NIR photon harvesting: progressive engineering of catalysts for solar-powered environmental purification and fuel production, Adv. Mater. 30 (2018) 1802894.

[21] R. Ma, J. Sun, D.H. Li, J.J. Wei, Exponentially self-promoted hydrogen evolution by uni-source photo-thermal synergism in concentrating photocatalysis on co-catalyst-free P25 TiO_2, J. Catal. 392 (2020) 165–174.

[22] R. Ma, J. Sun, D.H. Li, J.J. Wei, Review of synergistic photo-thermo-catalysis: mechanisms, materials and applications, Int. J. Hydrog. Energy 45 (2020) 30288–30324.

[23] R. Ma, H. Su, J. Sun, D.H. Li, Z.W. Zhang, J.J. Wei, Concentrating photo-thermo-organized single-atom and 2D-raft Cu catalyst for full-spectrum solar harmonic conversion of aqueous urea and urine into hydrogen, Appl. Catal. B Environ. 315 (2022) 121493–121507.

[24] D.H. Li, J. Sun, R. Ma, J.J. Wei, High-efficient solar-driven hydrogen production by full-spectrum synergistic photo-thermo-catalytic methanol steam reforming with in-situ photoreduced Pt-CuO_x catalyst, J. Energy Chem. 71 (2022) 460–469.

[25] J.Q. Zhang, Y.G. Li, J.M. Sun, H.J. Chen, Y.Z. Zhu, X.L. Zhao, L.C. Zhang, S. J. Wang, H.Y. Zhang, X.G. Duan, L. Shi, S. Zhang, P. Zhang, Gu.S. Shao, M.B. Wu, S. B. Wang, H.Q. Sun, Regulation of energetic hot carriers on Pt/TiO_2 with thermal energy for photothermal catalysis, Appl. Catal. B Environ. 309 (2022), 121263.

[26] A. Durán, J.M. Monteagudo, I. Sanmartín, A. García-Díaz, Sonophotocatalytic mineralization of antipyrine in aqueous solution, Appl. Catal. B Environ. 138-139 (2013) 318–325.

[27] X.J. Li, S.Y. Zhao, X.G. Duan, H.Y. Zhang, S.Z. Yang, P.P. Zhang, S.P. Jiang, S. M. Liu, H.Q. Sun, S.B. Wang, Coupling hydrothermal and photothermal single-atom catalysis toward excellent water splitting to hydrogen, Appl. Catal. B Environ. 283 (2021), 119660.

[28] Y.P. Huang, Z.L. Li, K. Yao, C.C. Chen, C.Y. Deng, Y.F. Fang, R.P. Li, H.L. Tian, Suppressing toxic intermediates during photocatalytic degradation of glyphosate by controlling adsorption modes, Appl. Catal. B Environ. 299 (2021), 120671.

[29] L.L. Long, L.L. Su, W. Hu, S.H. Deng, C. Chen, F. Shen, M. Xu, G.X. Huang, G. Yang, Micro-mechanism of multi-pathway activation peroxymonosulfate by copper-doped cobalt silicate: the dual role of copper, Appl. Catal. B Environ. 309 (2022), 121276.

[30] Z. Zheng, B. Huang, J. Lu, Z. Wang, X. Qin, X. Zhang, Y. Dai, M.H. Whangbo, Hydrogenated titania: synergy of surface modification and morphology improvement for enhanced photocatalytic activity, Chem. Commun. 48 (2012) 5733–5735.

[31] Z. Wang, C. Yang, T. Lin, H. Yin, P. Chen, D. Wan, F. Xu, F. Huang, J. Lin, X. Xie, M. Jiang, Visible-light photocatalytic, solar thermal and photoelectrochemical properties of aluminium-reduced black titania, Energy Environ. Sci. 6 (2013) 3007–3014.

[32] X. Chen, L. Liu, P.Y. Yu, S.S. Mao, Increasing solar absorption for photocatalysis with black hydrogenated titanium dioxide nanocrystals, Science 331 (2011) 746–750.

[33] A. Sinhamahapatra, J.P. Jeon, J.S. Yu, A new approach to prepare most active and stable black titania for visible light-assisted hydrogen production, Energy Environ. Sci. 8 (2015) 3539–3544.

[34] X.B. Li, W.W. Wang, F. Dong, Z.Q. Zhang, L. Han, X.D. Luo, J.T. Huang, Z.J. Feng, Z. Chen, G.H. Jia, T.R. Zhang, Recent advances in noncontact external-field-assisted photocatalysis: from fundamentals to applications, ACS Catal. 11 (2021) 4739–4769.

[35] Q. Jia, P.K. Nguyen, Z.H. Gu, X.J. Zhang, M. Liu, X.F. Tian, L. Ma, L. Gong, X. Mu, Y.L. Chang, N-doped bismuth molybdate decorated with Pt nanoparticles removal azo dyes efficiently via the synergistic effect of adsorption and photocatalysis, J. Alloys Compd. 863 (2021) 158336–158350.

[36] J. Park, S. Lee, H.E. Kim, A. Cho, S. Kim, Y. Ye, J.W. Han, H. Lee, J.H. Jang, J. Lee, Investigation of the support effect in atomically dispersed Pt on WO_{3-x} for utilization of Pt in the hydrogen evolution reaction, Angew. Chem. Int. Ed. 58 (2019) 16038–16042.

[37] E. Carter, A.F. Carley, D.M. Murphy, Evidence for O^{2-} radical stabilization at surface oxygen vacancies on polycrystalline TiO_2, J. Phys. Chem. C 111 (2007) 10630–10638.

[38] A. Kumar, V. Krishnan, Vacancy engineering in semiconductor photocatalysts: implications in hydrogen evolution and nitrogen fixation applications, Adv. Funct. Mater. 31 (2021) 2009807–2009840.

[39] J.X. Yang, W.B. Yu, C.F. Li, W.D. Dong, L.Q. Jiang, N. Zhou, Z.P. Zhuang, J. Liu, Z. Y. Hu, H. Zhao, Y. Li, L.H. Chen, J.G. Hu, B.L. Su, PtO nanodots promoting Ti_3C_2 MXene in-situ converted Ti_3C_2/TiO_2 composites for photocatalytic hydrogen production, Chem. Eng. J. 420 (2021), 129695.

[40] J. Xiao, S. Liu, N. Tian, Z.Y. Zhou, H.X. Liu, B.B. Xu, S.G. Sun, Synthesis of convex hexoctahedral Pt micro/nanocrystals with high-index facets and electrochemistry-mediated shape evolution, J. Am. Chem. Soc. 135 (2013) 18754–18757.

[41] C. Xiao, N. Tian, W.Z. Li, X.M. Qu, J.H. Du, B.A. Lu, B.B. Xu, Z.Y. Zhou, S.G. Sun, Shape transformations of Pt nanocrystals enclosed with high-index facets and low-index facets, CrystEngComm 23 (2021) 6655–6660.

[42] Y. Wang, P. Han, X. Lv, L. Zhang, G. Zheng, Defect and interface engineering for aqueous electrocatalytic CO_2 reduction, Joule 2 (2018) 2551–2582.

[43] H.S.Y. Fang, Z.X. Sun, Y.H. Hu, Insights into the thermo-photo catalytic production of hydrogen from water on a low-cost NiO_x-loaded TiO_2 catalyst, ACS Catal. 9 (2019) 5047–5056.

[44] W.X. Chen, J.J. Pei, C.T. He, J.W. Wan, H.L. Ren, Y.Q. Zhu, Y. Wang, J.C. Dong, S. B. Tian, W.C. Cheong, S.Q. Lu, L.R. Zheng, X.S. Zheng, W.S. Yan, Z.B. Zhuang, C. Chen, Q. Peng, D.S. Wang, Y.D. Li, Rational design of single molybdenum atoms anchored on N-doped carbon for effective hydrogen evolution reaction, Angew. Chem. Int. Ed. 129 (2017) 16302–16306.

[45] Y. Zheng, Y. Jiao, Y. Zhu, L.H. Li, Y. Han, Y. Chen, M. Jaroniec, S.Z. Qiao, High electrocatalytic hydrogen evolution activity of an anomalous ruthenium catalyst, J. Am. Chem. Soc. 138 (2016) 16174–16181.